12th International Symposium on Turbulence and Shear Flow Phenomena (TSFP12)
Osaka, Japan (Online), July 19-22, 2022

PERMEABILITY EFFECTS ON TURBULENT CHANNEL FLOWS OVER POROUS RIB-ROUGHNESS

Y. Okazaki
Department of Mechanical Engineering
Osaka Prefecture University, Japan
okazaki@htlab.me.osakafu-u.ac.jp

Y. Takase
Department of Mechanical Engineering
Osaka Prefecture University, Japan
takase@htlab.me.osakafu-u.ac.jp

Y. Kuwata
Department of Mechanical Engineering
Osaka Metropolitan University, Japan
kuwata@me.osakafu-u.ac.jp

K. Suga
Department of Mechanical Engineering
Osaka Metropolitan University, Japan
suga@me.osakafu-u.ac.jp

ABSTRACT

To understand permeable roughness effects on turbulence, PIV measurements of turbulent channel flows over porous roughness are carried out. We consider fully developed turbulent channel flows over porous bottom walls with transverse square porous-ribs whose heights are 10% of the channel height. The considered ratios of the rib spacing w to the rib height k are w/k =1, 3, 7, 9 and 19. The porous ribs are also made of the same material as that for the bottom wall. Three kinds of metallic foam materials are applied as the porous media. The permeability of the most permeable medium is approximately five times as large as that of the least permeable one while the porosities of all three media are 0.95. Solid impermeable rib-roughness cases are also measured for comparison. The measured flows are in the range of the bulk Reynolds numbers of 5000–20000. At $w/k = 1$, the levels of turbulence quantities and the drag coefficient become larger as the permeability increases while such a trend becomes unclear at $w/k = 3$ and a reversed trend is seen at $w/k \geq 7$. At a higher permeability, however, it is found that the sensitivity to the rib spacing on the profiles of the turbulence quantities and the drag coefficient is weakened. Even at a lower permeability, turbulence tends to be less sensitive to the rib spacing at $w/k > 3$. The equivalent sand grain roughness height hence follows these trends. It is found that there is an almost linear correlation between the zero-plane displacement and the hydraulic roughness scale of the logarithmic law of the mean velocity over the roughness. It is also shown that the effective displacement, which is introduced for isolating the permeability effects, and the von Kármán constant have reasonable correlations with the permeability Reynolds numbers.

INTRODUCTION

Fundamental knowledge on rough wall turbulence accumulated by many studies has been summarized several times in review articles (e.g., Raupach *et al.*, 1991; Jiménez, 2004; Flack & Schultz, 2010; Piomelli, 2018; Chung *et al.*, 2021). From those studies, to characterise rough wall turbulence we recognize that there are many parameters as described in the latest review by Chung *et al.* (2021). In case of very high roughness, the surfaces such as vegetation and urban canopies are sometimes treated as porous media (e.g., Lin *et al.*, 2012; Huang *et al.*, 2013; Rubol *et al.*, 2018; Ming *et al.*, 2021). The difference between the definitions of porous and rough walls hence sometimes becomes ambiguous. The important parameters for porous media are however porosity (void fraction) and permeability (Whitaker, 1986, 1996). The permeability is a macroscopic measure of porous media and it can be considered to include the effects of all the aforementioned topographical roughness parameters on drag through porous structures.

For flows around porous media, permeability plays a determinate role for drag. Zippe & Graf (1983); Kuwata & Suga (2016*a*) confirmed that overall friction loss was greater than that over equivalent impermeable rough surfaces. By the measurements of the momentum flux across the porous interface, Pokrajac & Manes (2009) recognised that due to the permeability, the momentum exchange process was enhanced near the porous interface. By systematic direct numerical simulations (DNSs) and particle-image-velocimetry (PIV) measurements (Breugem *et al.*, 2006; Kuwata & Suga, 2016*a*; Suga *et al.*, 2011, 2017), turbulence over permeable walls was investigated in detail and it was confirmed that due to the weakened wall blocking effects by the wall permeability, the wall-normal fluctuating velocity was not completely damped leading to the high drag over the permeable walls. By analysing the DNS data, Kuwata & Suga (2016*b*) confirmed that while the main source of the turbulent energy was the mean shear over the porous layer, the contribution from the dispersion became dominant inside the porous layer.

To the best of the authors' knowledge, however, except for the study by the present authors' group (Okazaki *et al.*, 2020), there has been no systematic study that reports turbulence over rib-roughened porous walls in the literature. To discuss the porous roughness effect, Okazaki *et al.* (2020) carried out PIV measurements of turbulent flows over rib-roughened porous walls. Their case was for regularly aligned square ribs at $w/k = 9$ where w and k are the rib-spacing and the rib-height, respectively. Following Perry *et al.* (1969), it is widely accepted that "impermeable" wall roughness is categorized into two types: k- and d-types and $w/k = 9$ is in the k-type roughness regime. The experiments confirmed that as the permeability increased, the recirculation region formed behind the rib became smaller and moved down into the porous wall leading to weakened turbulence and decreased hydraulic

roughness heights. The turbulent drag hence became small as the permeability increased. It was however still unknown whether such a trend was maintained in other w/k cases. Also, there was no knowledge on how the permeability affected the rib-spacing effects on turbulence.

Therefore, to further explore the above-mentioned trends and to understand turbulence over permeable roughness, this study has carried out PIV measurements of turbulent flows in the porous rib-roughened channels of w/k =1–19 at a range of the Reynolds numbers: Re_b =5000–20000. We apply three kinds of metallic foam porous media of the porosity of 0.95, but their permeabilities and mean pore diameters are significantly different. These porous media are considered to be isotropic media.

EXPERIMENTAL METHOD

Fig.1 shows our flow facility. The PIV experimental setup is the same as that used in our previous studies (e.g., Suga *et al.*, 2010). It consists of a conditioning section and driving and test sections whose cross-sectional size is 0.06 m (height) $\times$ 0.3 m (width) as shown in Fig.1(a). Rib-roughened porous slabs fill the bottom half of these sections so that the clear channel height is H=0.03 m. Turbulent flows are fully developed through the driving section ($100H$ long) and enter the test section. As seen in Fig.1(b), the measurements are conducted at the symmetry plane of the channel where two dimensionality is confirmed (Suga *et al.*, 2013). This study applies three kinds of metallic foam porous media of porosity $\varphi = 0.95$ as listed in Table 1. The porosity is defined as the ratio of the intrinsic (fluid phase) and the superficial (total phase) volumes of porous media. The permeabilities are obtained using the Darcy-Forchheimer equation:

$$-\frac{\Delta P}{\Delta x} = \frac{\mu U_d}{K} + \frac{\rho C^F}{K} U_d^2, \tag{1}$$

where $\frac{\Delta P}{\Delta x}, \mu, \rho, C^F$ and U_d are the pressure gradient in streamwise direction, fluid viscosity, density, the Forchheimer coefficient and the mean velocity, respectively. The mean pore diameter D_p was obtained by averaging the equivalent circle areas converted from the measured cross section areas of pores. The most permeable medium #13m has approximately five times larger permeability than the least permeable one #30m. Accordingly, we call #13m, #20m and #30m "high", "medium" and "low" permeable media, respectively. On their surface, square-shaped porous ribs whose height $k = 3$ mm are set with the same spacings of $w/k = 1, 3, 7, 9, 19$ as shown in Fig.1(c). Note that the porous ribs are made of the same material as that for the bottom wall and hence the mean pore diameter of the most permeable medium is 77% of the rib height. To compare the data, the solid impermeable cases are also measured. The measured Reynolds number range is $\mathrm{Re}_b = 5000$–20000. The Reynolds number is defined as $\mathrm{Re}_b = U_b H/\nu$ where ν is the fluid kinematic viscosity and U_b is the bulk velocity that is calculated by integrating the measured mean velocities from the rib-bottom position to the top wall.

Table 1. Characteristics of the porous media; φ: porosity, K: permeability, D_p: mean pore diameter.

Porous Med.	φ	K(mm^2)	D_p (mm)
#30m		0.007	0.8
#20m	0.95	0.013	1.7
#13m		0.033	2.3

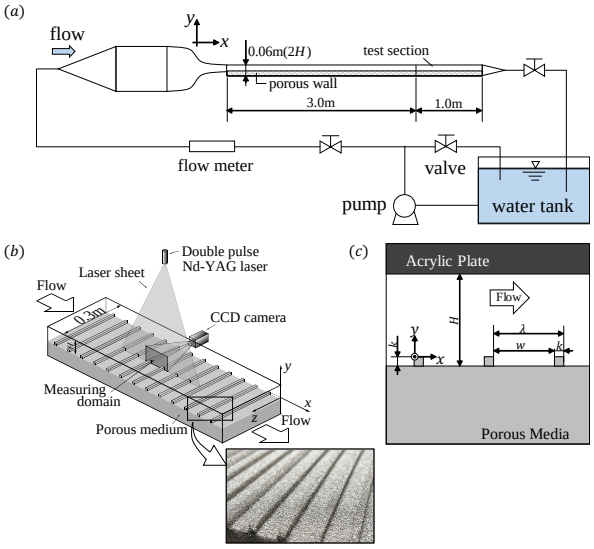

Figure 1. Experimental setup: (a) schematic view of the flow facility, (b) overall view of the test section, (c) side view of the test section.

RESULTS and DISCUSSION

Streamlines

To illustrate the general flow patterns, Figs.2 and 3 show streamlines by plotting contour lines of the stream functions calculated with the measured mean velocity distributions at $\mathrm{Re}_b \simeq 15000$. In the low permeability case (case #30m), although the confined recirculation is still observed between the ribs at $w/k = 1$, the centre of the recirculation bubble shifts downstream. When w/k becomes large, the recirculation tends to relax and seems to submerge into the bottom porous wall. In the high permeability case (case #13m), the trend observed advances and almost no recirculation bubbles can be seen. This is significant at $w/k = 1$ while the flow patterns at $w/k = 7$ look similar to those of case #30m. Obviously, as the permeability increases, the flows through the ribs increase leading to the relaxation of the recirculating flows. The bottom wall permeability also weakens the recirculation by the by-passing flows below the ribs and it also allows penetration of the flows between the ribs.

Turbulence distribution

To generally observe the turbulence trends, Figs. 4 and 5 show spatial distributions of in-plane turbulent kinetic energy $\overline{q_{xy}^2}/2 = (\overline{u'^2} + \overline{v'^2})/2$ normalized by the bulk mean velocity U_b at $\mathrm{Re}_b \simeq 15000$. Here, $\overline{u'^2}$ and $\overline{v'^2}$ are the streamwise and wall-normal Reynolds normal stresses, respectively.

It is seen that the turbulence level of the low permeability case (case #30m) at $w/k = 1$ shown in Fig. 4 (a) is significantly lower than those of the other cases. As w/k becomes larger, generation of turbulence is enhanced above the shear layers as seen in Fig. 4 (b) and (c). This trend is consistent with that shown for the Reynolds shear stress of impermeable cases by Cui *et al.* (2003). In the high permeability case (case #13m), as shown in Fig. 5, the general turbulence level at $w/k = 1$ is comparable to that at the larger w/k. This is because turbulence generation in the region near the rib top position ($y = 0$) increases significantly depending on the increase of the permeability as Fig. 5 (a) indicates. The increasing trend of turbulence level, however, is not monotonic and at $w/k = 7$ the general turbulence level looks slightly reduced as seen in Fig.

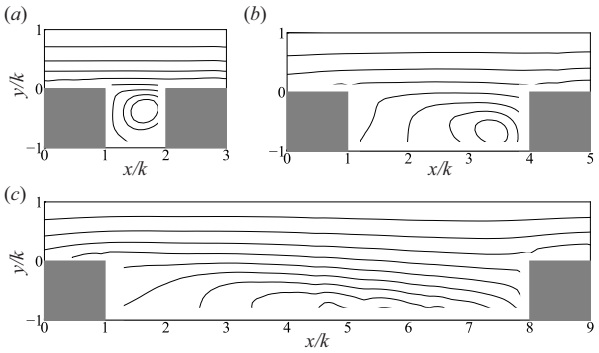

Figure 2. Streamlines in the low permeability case (case #30) at $\mathrm{Re}_b \simeq 15000$: (a) $w/k = 1$, (b) $w/k = 3$, (c) $w/k = 7$.

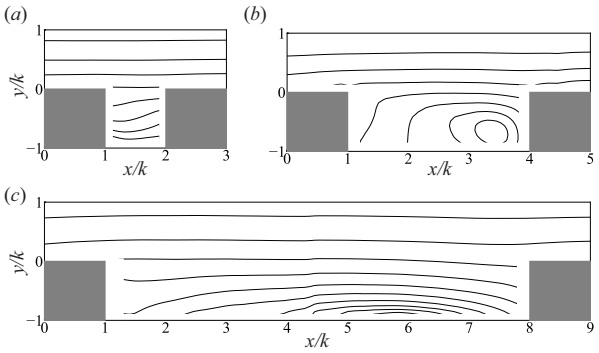

Figure 3. Streamlines in the high permeability case (case #13) at $\mathrm{Re}_b \simeq 15000$: (a) $w/k = 1$, (b) $w/k = 3$, (c) $w/k = 7$.

5 (c). More detailed turbulence trends are discussed focusing on each turbulence quantity in the following section.

Drag coefficient

Fig.6 shows the total drag coefficient $C_D = 2\tau_w/(\rho U_b^2)$ at $\mathrm{Re}_b \simeq 15000$, where τ_w is the total drag on the rib bottom. Here, τ_w is obtained by extrapolating total stress (sum of the Reynolds stress, viscous stress and dispersion stress) profile to the bottom porous wall at $y = -k$. The presently observed general trend of case solid agrees with the data of Leonardi *et al.* (2003) while the present values at $w/k = 3, 9$ are somewhat larger. In the present study, the peak appears around $w/k \simeq 9$, although the difference between the values of $w/k = 7$ and 9 is not significant.

The total drag coefficients C_D for the permeable cases show characteristic behaviours which correspond to the trends of turbulence quantities. Since the mean pore diameter of the high permeability case (case #13) is 77% of the rib height and its porosity is 0.95, its permeability is considered to be close to the maximum for the rib-roughened wall geometry. This implies that the range of the observed permeability (or pore-scale) dependent trends for turbulence quantities covers those of most permeable rib-roughness cases (from the impermeable to highest permeable cases). At $w/k = 1$, C_D of the low permeable case (case #30m) is significantly smaller than those of the medium and high permeability cases (cases #20m and #13m). As w/k increases, C_D of case #30m increases significantly up to $w/k = 3$ like in case solid. After catching up with those of the higher permeable cases, C_D of case #30m gradually increases toward $w/k = 9$, then turns to decrease slowly to $w/k = 19$. As the permeability increases, C_D increases at $w/k = 1$ while it seems to decrease at $w/k \geq 9$. This trend

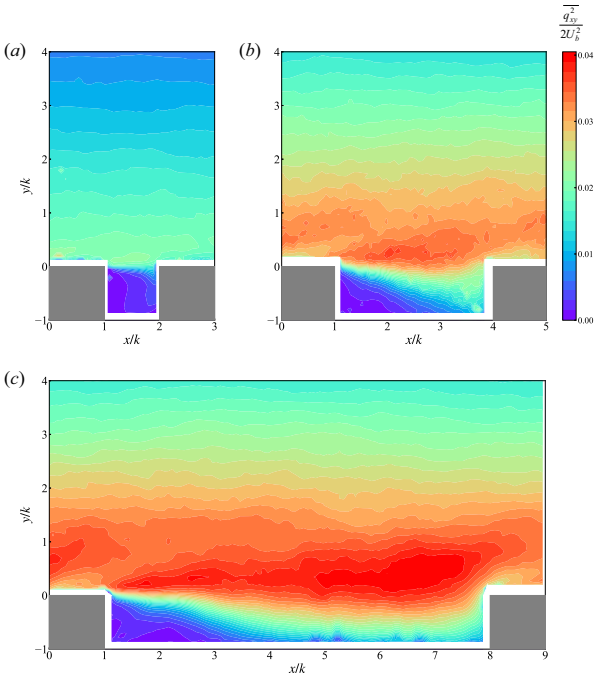

Figure 4. In-plane turbulent kinetic energy $\overline{q_{xy}^2}/2$ distributions in the low permeability case (case #30m) at $\mathrm{Re}_b \simeq 15000$: (a) $w/k = 1$, (b) $w/k = 3$, (c) $w/k = 7$.

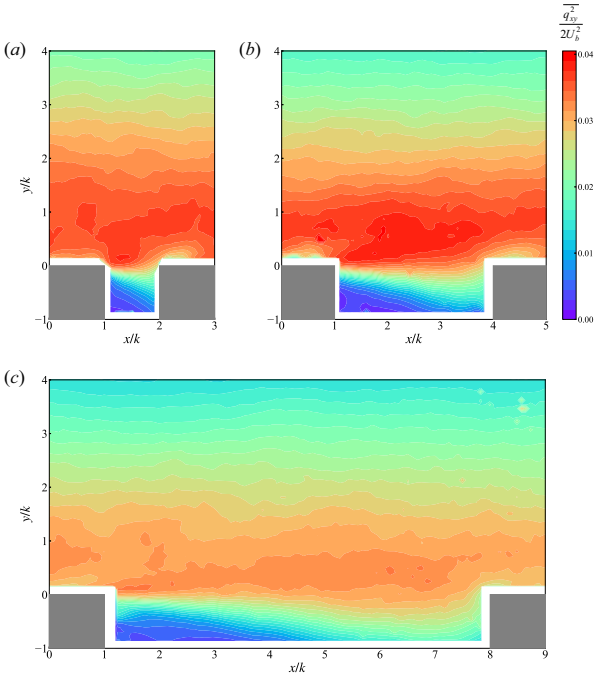

Figure 5. In-plane turbulent kinetic energy $\overline{q_{xy}^2}/2$ distributions in the high permeability case (case #13m) at $\mathrm{Re}_b \simeq 15000$: (a) $w/k = 1$, (b) $w/k = 3$, (c) $w/k = 7$.

is confirmed for all measured Reynolds numbers. The above observation suggests that as the permeability or the pore-scale increases, the d-type characteristics become weak and the transition to the k-type roughness takes place. Since the larger permeability and pore-scale reduce pressure drag of the rib roughness, turbulence tends to decrease gradually at the larger w/k as seen at $w/k > 9$.

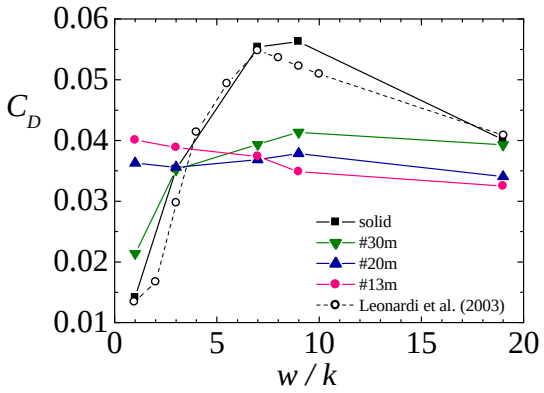

Figure 6. Drag coefficient at $\mathrm{Re}_b \simeq 15000$.

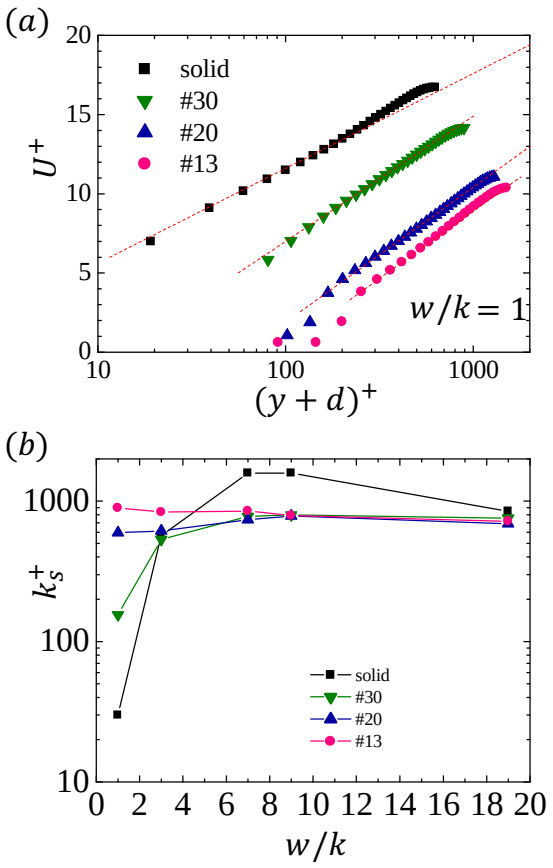

Figure 7. (a) Semi-logarithmic velocity profiles of $w/k = 1$ and (b) Equivalent sand grain roughness, at $\mathrm{Re}_b \simeq 15000$.

Roughness parameters

In the following, we discuss the mean velocity profiles of the logarithmic formula:

$$U^+ = \kappa^{-1} \ln \frac{y+d}{h}, \tag{2}$$

with d and h which are the zero-plane displacement and the roughness scale, respectively. In the literature, discussions of flows over porous media and canopies have applied this equation. The method described in Breugem *et al.* (2006); Suga *et al.* (2010) is applied to fitting the profiles to the equation 2

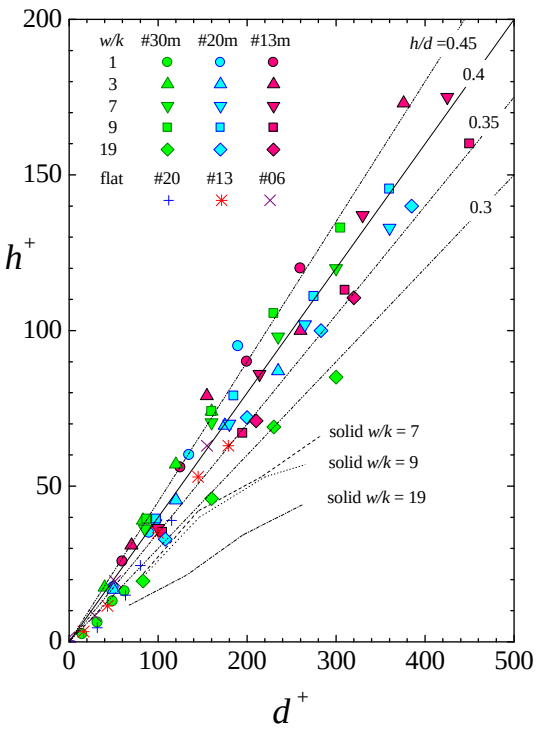

Figure 8. Correlation between roughness scale h and zero-plane displacement d. The data of the flat cases are from Suga *et al.* (2010).

for obtaining κ, d and h. Fig.7(a) shows velocity profiles in the semi-logarithmic chart and the fitted lines. Note that as reported in the previous studies (e.g., Breugem *et al.*, 2006; Suga *et al.*, 2010), the von Kármán constant becomes lower than 0.41. This suggests that the roughness function which normally denotes the downward shift of the semi-logarithmic velocity profile cannot be simply applied to the porous walled turbulence.

For the rough wall turbulence, another logarithmic formula:

$$U^+ = \kappa^{-1} \ln \frac{\hat{y}}{k_s} + 8.5, \tag{3}$$

may be applied with the equivalent sand grain roughness height k_s and the wall-normal distance $\hat{y}$ from the origin which should be determined empirically (Jiménez, 2004) and we apply $\hat{y} = y + d$. Consequently, coupling equations (2) and (3) we can convert h to the equivalent sand grain roughness k_s as $k_s = h \exp(8.5\kappa)$. Fig. 7(b) shows the w/k dependency of k_s^+ at $\mathrm{Re}_b \simeq 15000$. The overall trends are hence similar to those observed in the C_D profiles shown in Fig.6 while the decreasing trend by the increased permeability at $w/k \geq 9$ is not observed.

Among the parameters of the lag-law formula, we focus on the relation between d and h. Since both parameters are related to the surface geometry, there may be a relationship (Okazaki *et al.*, 2021). Fig.8 shows h vs. d for all measured Reynolds numbers including the plots for the flat porous wall cases of Suga *et al.* (2010). Note that porosities in Suga *et al.* (2010) were $\varphi \simeq 0.8$ and slightly smaller than the present one. While the plots are somewhat scattered, a generally reasonable correlation around $h/d = 0.4$ is seen for all the porous

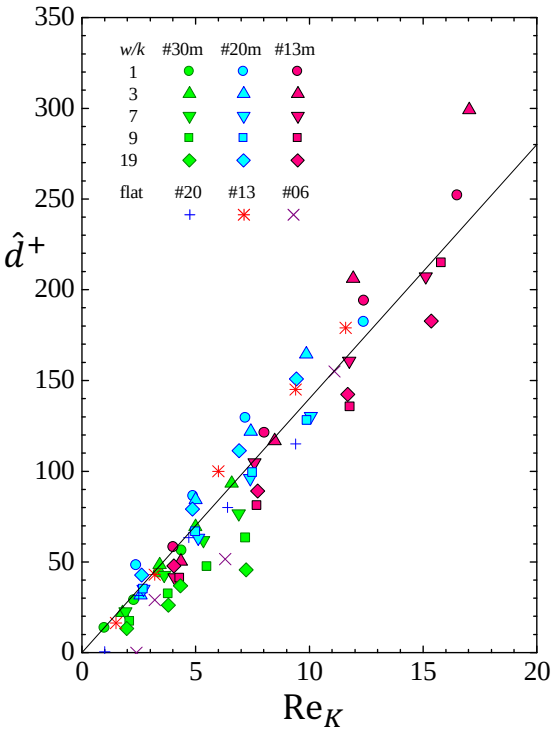

Figure 9. Distribution of the effective displacement $\hat{d}$ against the permeability Reynolds number Re_K. The thin solid black line denotes $\hat{d}^+ = 14\mathrm{Re}_K$.

cases. For the impermeable case (case solid), although a linear correlation may exist depending on w/k, the ratio of h/d is significantly smaller than 0.4. This implies that although h and d have an almost linear correlation, the ratio may change depending on the permeability and the roughness spacing.

Since d depends on both wall permeability and roughness geometry, following (Okazaki *et al.*, 2021), we introduce the effective displacement $\hat{d}$ to separate the effect of the roughness geometry as $\hat{d} = d - d_S$, where d_S denotes the zero-plane displacement of the corresponding impermeable case. To describe permeability effects on flow characteristics, the permeability Reynolds number, $\mathrm{Re}_K = u_* \sqrt{K}/\nu$, has been usually applied (e.g., Breugem *et al.*, 2006). Fig.9 hence shows the relation between $\hat{d}^+$ and Re_K. The flat porous wall cases are also included with $d_S = 0$. It is seen that all plots in Fig.9 distribute around the thin black line which denotes $\hat{d}^+ = 14\ \mathrm{Re}_K$. This indicates that generally, $\hat{d}^+$ has reasonable linear relationship with Re_K. It is noticeable that the wall permeability effect can be separated by simply subtracting the impermeable zero-plane displacement from the zero-plane displacement of porous roughness.

As for d_S, Fig.10 shows the presently obtained d_S and the results of Leonardi *et al.* (2003) who calculated d_S with the centroid of the moment of forces acting on the elements using the method of Jackson (1981). Note that $d_S/k = 0$ and 1 correspond to the rib-top and rib-bottom positions, respectively. The dashed curved line shows $d_S/k = (k - k_m)/k$, where $k_m = k/(k+w)$ is the mean roughness height. At the d-type roughness at $w/k < 3$, the present plots of d_S/k suggest that the line of Leonardi *et al.* (2003) is reasonable, while for the k-type roughness at $w/k \geq 7$, the present plots far deviate from the solid line but agree well with the dashed line. We thus suggest using the Jackson model for the d-type roughness but for

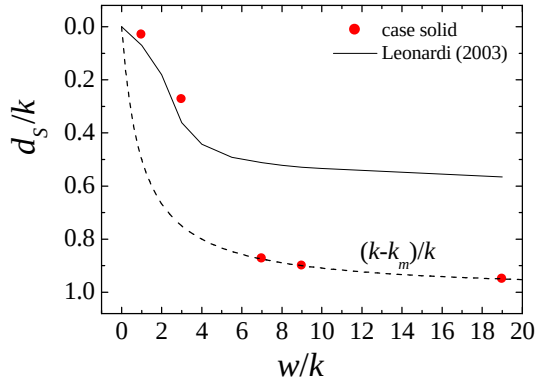

Figure 10. Zero-plane displacement for impermeable roughness. The solid line is from Leonardi *et al.* (2003) while the dashed line denotes the position of the mean roughness height.

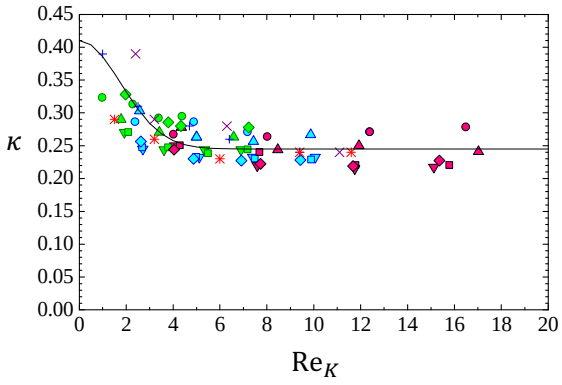

Figure 11. Distribution of κ against the permeability Reynolds number Re_K. Symbols are as in Fig. 9.

the k-type roughness we recommend applying the simple relation: $d_S = k - k_m$.

Considering the presently accumulated data, we try to find an empirical correlation formula for porous rib-roughness. Fig.11 shows the relation of κ to Re_K. It is seen that regardless of the rib spacing, κ distributes more or less around the thin solid lines which indicate the formula:

$$\kappa = \kappa_0 - A \exp[-(Re_K/B)^C] \tag{4}$$

with $\kappa_0 = 0.41$ and $A = 0.165$, $B = 2.5$ and $C = 2$. It is therefore noticeable that approximated values of all the parameters of log-law formulae can be estimated using Re_K and d_S. This is very helpful for engineering. Indeed, this strategy can be applied to wall functions for turbulence models in computational fluid dynamics codes which are routinely utilized for designing industrial devices.

CONCLUSIONS

To describe the effects of permeable roughness on turbulence, we have carried out PIV measurements of fully de-

veloped turbulent channel flows over three kinds of isotropic porous media with square-rib roughness at the bulk Reynolds numbers of 5000–20000. Since the flow rate through the ribs increases as the permeability increases, the recirculation bubbles between the ribs shift downstream and to the bottom wall. The change of the flow patterns at $w/k < 3$ enhances turbulence around the rib-top region. For the high permeability case, even at $w/k = 1$, it is observed that the enhanced rib permeability leads to the vanishment of the recirculation bubbles and the significant increase of turbulence over the ribs. At $w/k = 1$, because the permeability is considered to enhance the transition from the d-type to k-type roughness, the magnitude of turbulence becomes larger depending on the permeability. At $w/k > 3$, which is characterized as the k-type roughness for the impermeable case, the increase of turbulence by the permeability becomes unclear since the transition to the k-type is already completed. At $w/k \geq 7$, since the permeability reduces pressure drag of the rib roughness, the turbulence level reduces slightly as the permeability increases. These trends are reflected in the profiles of total drag and the equivalent sand grain roughness height. Since the permeability also enhances the transition to the fully rough regime, the Reynolds number effects on turbulence quantities tend to vanish at a higher Reynolds number. It is found that there are almost linear correlations between the zero-plane displacement d and the hydraulic roughness scale h of the logarithmic law of the mean velocity over the roughness. The ratio h/d however varies depending on the permeability and the rib spacing. For the presently measured permeable cases at $w/k \leq 9$, most plots distribute around $h/d = 0.4$. It is confirmed that the wall permeability effect on the zero-plane displacement can be separated by simply subtracting the impermeable zero-plane displacement from the zero-plane displacement of porous roughness. The effective displacement, which is obtained by this procedure, has an approximately linear correlation to the permeability Reynolds number. In the permeable cases, the von Kármán constant becomes smaller than 0.41 and varies significantly depending on the permeability and the rib spacing. Its plots suggest there is a reasonable correlation with the permeability Reynolds number.

REFERENCES

Breugem, W. P., Boersma, B. J. & Uittenbogaard, R. E. 2006 The influence of wall permeability on turbulent channel flow. *J. Fluid Mech.* **562**, 35–72.

Chung, Daniel, Hutchins, Nicholas, Schultz, Michael P. & Flack, Karen A. 2021 Predicting the drag of rough surfaces. *Ann. Re. Fluid Mech.* **53** (1), 439–471.

Cui, J., Patel, V. C. & Lin, C.-L. 2003 Large-eddy simulation of turbulent flow in a channel with rib roughness. *Int. J. Heat Fluid Flow* **24**, 372–388.

Flack, K. A. & Schultz, M. P. 2010 Review of hydraulic roughness scales in the fully rough regime. *J. Fluids Engng.* **132**, 041203.

Huang, C. W., Lin, M., Khlystov, A. & Katul, G. 2013 The effects of leaf area density variation on the particle collection efficiency in the size range of ultrafine particles (UFP). *Environ. Sci. Technol.* **47**, 607–615.

Jackson, P. S. 1981 On the displacement height in the logarithmic velocity profile. *J. Fluid Mech.* **111**, 15–25.

Jiménez, J. 2004 Turbulent flows over rough walls. *Annu. Rev. Fluid Mech.* **36** (1), 173–196.

Kuwata, Y. & Suga, K. 2016*a* Lattice Boltzmann direct numerical simulation of interface turbulence over porous and rough walls. *Int. J. Heat Fluid Flow* **61**, 145–157.

Kuwata, Y. & Suga, K. 2016*b* Transport mechanism of interface turbulence over porous and rough walls. *Flow Turb.Combust.* **97**, 1071–1093.

Leonardi, S., Orlandi, P., Smalley, R. J., Djenidi, L. & Antonia, R. A. 2003 Direct numerical simulations of turbulent channel flow with transverse square bars on one wall. *J. Fluid Mech.* **491**, 229–238.

Lin, M., Katul, G. & Khlystov, A. 2012 A branch scale analytical model for predicting the collection efficiency of ultrafine particles. *Atmos. Environ.* **51**, 293–302.

Ming, Tingzhen, Lian, Shengnan, Wu, Yongjia, Shi, Tianhao, Peng, Chong, Fang, Yueping, de Richter, Renaud & Wong, Nyuk Hien 2021 Numerical investigation on the urban heat island effect by using a porous media model. *Energies* **14**, 4681.

Okazaki, Y., Shimizu, A., Kuwata, Y. & Suga, K. 2020 Turbulence characteristics over k-type rib roughened porous walls. *Int. J. Heat Fluid Flow* **82**, 108541.

Okazaki, Y., Takase, Y., Kuwata, Y. & Suga, K. 2021 Describing characteristic parameters of turbulence over two-dimensional porous roughness. *J. Therm. Sci. Tech.* **16**, JTST0027.

Perry, A. E., Schofield, W. H. & Joubert, P. N. 1969 Rough wall turbulent boundary layers. *J. Fluid Mech.* **37**, 383–413.

Piomelli, U. 2018 Recent advances in the numerical simulation of rough-wall boundary layers. *Phys. Chem. Earth* p. in press.

Pokrajac, D. & Manes, C. 2009 Velocity measurements of a free-surface turbulent flow penetrating a porous medium composed of uniform-size spheres. *Transp. Porous, Med.* **78**, 367–383.

Raupach, M. R., Antonia, R. A. & Rajagopalan, S. 1991 Rough-wall turbulent boundary layers. *Appl. Mech. Rev.* **44**, 1–25.

Rubol, Simonetta, Ling, Bowen & Battiato, Ilenia 2018 Universal scaling-law for flow resistance over canopies with complex morphology. *Sci. Rep.* **8**, 4430.

Suga, K., Matsumura, Y., Ashitaka, Y., Tominaga, S. & Kaneda, M. 2010 Effects of wall permeability on turbulence. *Int. J. Heat Fluid Flow* **31**, 974–984.

Suga, K., Mori, M. & Kaneda, M. 2011 Vortex structure of turbulence over permeable walls. *Int. J. Heat Fluid Flow* **32**, 586–595.

Suga, K., Nakagawa, Y. & Kaneda, M. 2017 Spanwise turbulence structure over permeable walls. *J. Fluid Mech.* **822**, 186–201.

Suga, K., Tominaga, S., Mori, M. & Kaneda, M. 2013 Turbulence characteristics in flows over solid and porous square ribs mounted on porous walls. *Flow Turb. Combust.* **91**, 19–40.

Whitaker, S. 1986 Flow in porous media I: A theoretical derivation of Darcy's law. *Transp. Porous Med.* **1**, 3–25.

Whitaker, S. 1996 The Forchheimer equation: A theoretical development. *Transp. Porous Med.* **25**, 27–61.

Zippe, H. J. & Graf, W. H. 1983 Turbulent boundary-layer flow over permeable and non-permeable rough surfaces. *J. Hydraul. Res.* **21**, 51–65.